Advances in Science and Technology Research Journal

Advances in Science and Technology Research Journal, 2026, 20(9), 195–208
https://doi.org/10.12913/22998624/221835
ISSN 2299-8624, License CC-BY 4.0

Received: 2026.03.27
Accepted: 2026.07.10
Published: 2026.08.01

Effect of combustible gas stream interaction on the static strength of fibre-reinforced composites

Robert Szczepaniak[1*], Julian Jabłczyński[2], Paweł Przybyłek[1], Joanna Masiewicz[1], Japhet Noubiap Ngouobe[3]

[1] Faculty of Aviation, Polish Air Force University, ul. Dywizjonu 303 No. 35, 08-521 Dęblin, Poland
[2] LOT Polish Airlines, ul. Komitetu Obrony Robotników 43, 02-146 Warsaw, Poland
[3] Laboratory of Energy, Water, and Environment, National Advanced School of Engineering of Yaoundé, P.O. Box 8390, Yaounde, Cameroon
* Corresponding author's e-mail: r.szczepaniak@law.mil.pl

ABSTRACT

The aim of this study was to evaluate the effect of short-term thermal exposure on the mechanical performance of a hybrid composite reinforced with carbon and aramid fibres. Composite panels were manufactured using the vacuum bagging technique and subsequently machined into specimens for puncture resistance, tensile, and three-point bending tests. The results showed a progressive reduction in mechanical properties relative to the unexposed reference state, indicating thermal degradation of the composite structure. The material exhibited good thermal insulation capability, particularly when heated from the aramid side. The influence of fibre type was found to be significant: the specimens exposed from the aramid fibre side retained higher puncture resistance and tensile performance compared to those exposed from the carbon fibre side, suggesting greater thermal stability of aramid fibres under the tested conditions. In contrast, bending strength showed the highest sensitivity to thermal exposure, with a substantial decrease relative to the initial (unexposed) values. Microscopic analyses confirmed that the observed mechanical degradation was associated with matrix decomposition, delamination, and microcrack formation. The obtained results contribute to a better understanding of the behaviour of hybrid composites under thermal loading and may support the design of structural materials for the applications requiring both load-bearing capacity and resistance to elevated temperatures. The results obtained are applied in the design of structural components used in the aerospace, automotive, and defense industries, where materials are exposed to high temperatures and fire. They can also be used in the development of protective systems, such as thermal shields and ablative coatings. Furthermore, this research supports the development of more resilient composites for use in special-purpose vehicles and infrastructure exposed to extreme operating conditions.

Keywords: tree-point bending, static tensile, mechanical degradation, delamination.

INTRODUCTION

Ablation is a complex phenomenon of heat and mass transfer that leads to irreversible structural and chemical changes in a material. This phenomenon is initiated and sustained by the influx of thermal energy from external sources, and its course involves both physical transformations as well as chemical reactions occurring within the material. In the physical description of ablation, several characteristic regions that jointly determine its progression can be distinguished [1–3]:

- the ablation surface, constituting the interface between the gaseous and solid phases,
- the ablation layer, located between the ablation surface and the ablation front,
- the ablation front, separating the transformation zone from the unaffected material,
- the virgin material, which has not yet been exposed to thermal influence.

Heating occurs at the ablation surface, whereas the principal chemical reactions take place within the ablation layer. These include a wide

range of phenomena, such as pyrolysis and chemical decomposition of the material, thermochemical transformations of decomposition products in the solid and gaseous phases, reactions between decomposition products present in different states of aggregation, phase transformations of components that do not undergo decomposition, as well as reactions occurring in the liquid phase [3–6].

To improve the effectiveness of thermal protection, polymer ablative composites are increasingly used, in which conventional resins such as epoxy or phenolic resins serve as the matrix. The influence of matrix type and its modification on the ablative and mechanical properties of composites is the subject of intensive research conducted using both numerical and experimental methods [7–10].

An important direction of development is also the reinforcement of composites with fibres (e.g., aramid or carbon fibres) and the incorporation of functional additives, including nanopowders and ceramic powders, aimed at improving thermal resistance and structural stability of the composite [11–14]. Due to operational requirements, additives used in ablative composites must also meet tribological and mechanical criteria. Consequently, studies are conducted on wear, friction, and material behaviour under dynamic conditions, as well as analyses of changes in thermophysical parameters over a wide temperature range [15–18].

Examples of effective solutions include honeycomb structures reinforced with aramid fibres and filled with phenolic foams, which exhibit high efficiency in thermal protection applications [19–21]. Increasing interest is also focused on the use of phase change materials (PCMs) as additives to ablative composites. Their presence enables temporary storage of thermal energy during phase transformation, which may potentially reduce material temperature and slow down degradation processes [1, 13, 22].

Although the application of PCMs in the composites intended for high-temperature operation is still relatively poorly understood, available studies include both fabrication methods for such materials and analyses of their thermophysical properties and ablative behaviour [23–25].

The literature reports studies on the mechanical properties of advanced composites based on carbon fibres and phthalonitrile resin, which show significant potential for aerospace applications [26]. It has also been demonstrated that the degradation of carbon fibres at elevated temperatures is the primary factor responsible for the reduction in mechanical strength, which is an important and often underestimated finding [27]. Further studies have investigated the influence of fibre orientation and heat flux on the residual (post-fire) load-bearing properties of CFRP laminates. The aim was to achieve a better understanding of material behaviour after thermal exposure, which is crucial for assessing the suitability of laminates with different fibre architectures in load-bearing structures [28]. Moreover, it has been shown that modifying CF/PN composites by incorporating CuO nanoparticles significantly improves their thermal resistance and mechanical performance, even after exposure to very high temperatures [29].

In light of the above, the objective of this study was to determine the effect of short-term flame exposure on the mechanical properties of a hybrid composite reinforced with carbon and aramid fibres. In particular, the study focused on analysing changes in material strength as a function of high-temperature exposure time and heating direction (from the carbon and aramid fibre sides). The aim of the research was also to identify the dominant mechanisms of structural degradation and to evaluate the ability of a composite to maintain mechanical integrity under short-term thermal loading.

MATERIALS AND METHODS

The study examined a layered polymer composite hybrid-reinforced with carbon and aramid fibres, intended for structural applications under elevated thermal loads. The selection of materials was intended to replicate the configuration of laminates used in aerospace structures, where a combination of high stiffness, impact resistance, and thermal resistance is required. The composite was fabricated as a nine-layer laminate with the following configuration:

$$[C/A/A]_3 \quad (1)$$

where: C – carbon fabric (plain weave GG 240, 200 g/m²), A – aramid fabric (twill weave STYLE 140 2/2, 110 g/m²).

The L285/H285 resin–hardener system (R&G, Germany), certified for aerospace applications, was used as the matrix. It is a low-viscosity

epoxy resin designed for structural lamination, characterized by high fibre adhesion and dimensional stability up to a glass transition temperature (Tg) of approximately 80–90 °C. The composite panels were manufactured using vacuum bagging at a pressure of 0.8 bar, ensuring the elimination of air bubbles. The composites were cured at room temperature for 24 hours. The final thickness of the panels after processing was approximately 2.0–2.6 mm. Specimens were cut from the panels (Figure 1) using a waterjet method in accordance with the relevant standards (Table 1).

The specimens were labelled with codes such as R.15.W.1, where:

- R – test type (tensile),
- 15 – flame exposure time in seconds divided by 3 for first and second batch (15 and 30) or 4 for the last batch of samples (60)
- W – carbon side (A – aramid side),
- 1 – specimen number.

The thermal tests were conducted using a propane–butane burner (heat output of approximately 43 MJ/kg). The specimens were heated from a distance of 35 mm for 5–15 s. The objective was to simulate short-term fire exposure, such as that occurring in the thermal shielding of aircraft components or military vehicles. Temperature measurements were performed using:

- a laser pyrometer (heated side),
- 18 K-type thermocouples (opposite side).

Following thermal exposure, mechanical tests were carried out:

- puncture resistance – Instron CEAST 9340 drop-weight impact tester, impact energy of 5 J,
- static tensile testing – Zwick/Roell Z100 testing machine,
- three-point bending – Zwick/Roell Z5.0 testing machine, support span of 50 mm.

Table 1. Standards and dimensions of test specimens for mechanical testing

Test type	Standard	Dimensions
Three-point bending	DIN EN ISO 178	80 × 10 mm
Tensile testing	PN-EN ISO 6892-1	250 × 25 mm
Impact strength	ISO 6603	60 × 80 mm

Subsequently, surface analyses were performed:

- surface profilometry – FRT100,
- scanning electron microscopy (SEM) and optical microscopy – structural degradation analysis using an Olympus BX53M+ optical microscope and a Hitachi TM3030Plus scanning electron microscope.

RESULTS

The following section presents the results of temperature measurements during exposure to a stream of flammable gases, as well as the results of mechanical tests performed on the specimens after thermal degradation. The analysis focuses on changes in mechanical properties as a function of heating time and the surface exposed to thermal loading (carbon or aramid side).

Temperature distribution in the specimens during heating

During the tests (Figures 2–4), a non-uniform temperature distribution was observed between

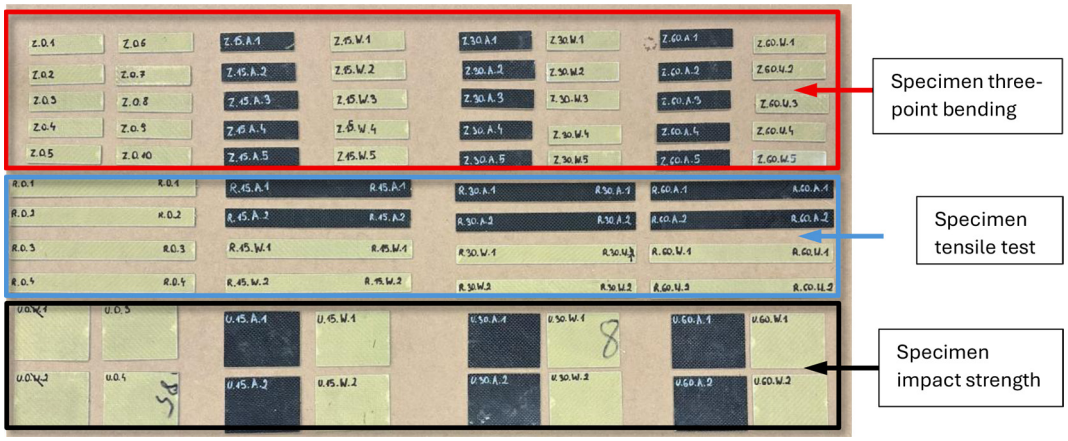

Figure 1. Specimens prepared for research

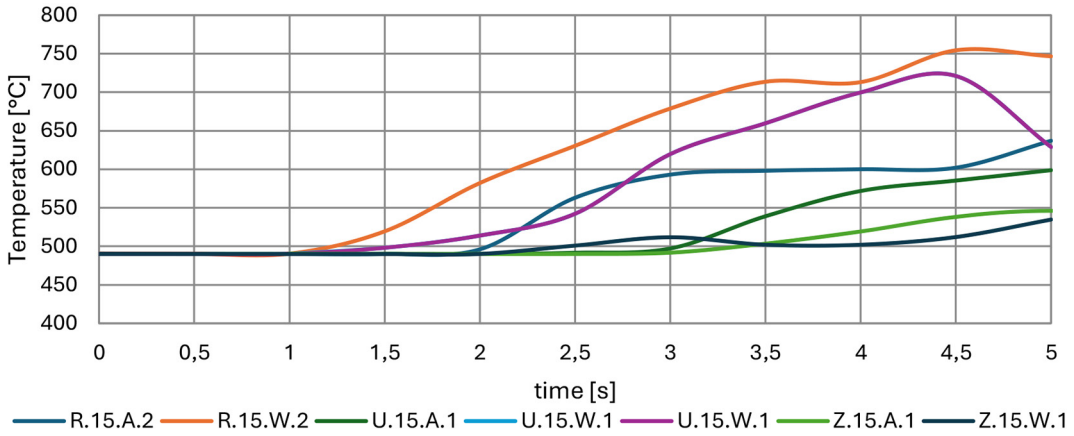

Figure 2. Results of surface temperature measurements of the sample during 5 seconds of heat flux exposure

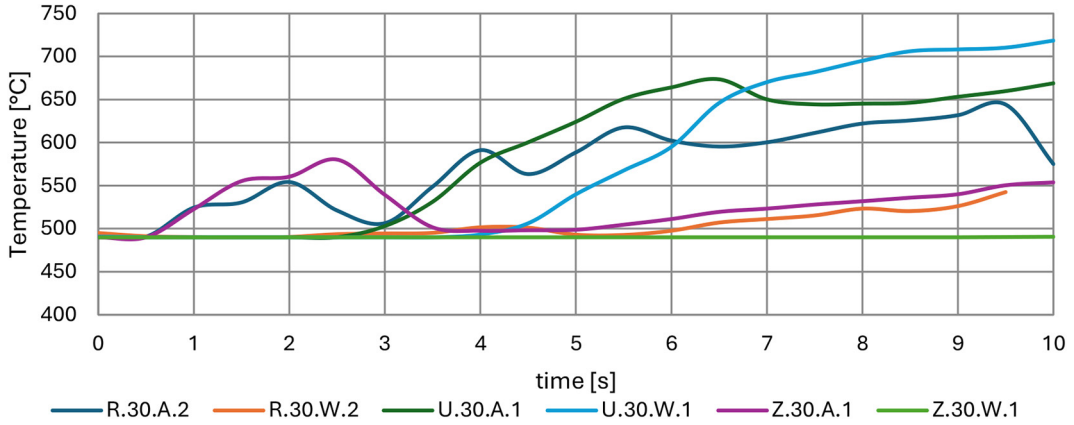

Figure 3. Results of surface temperature measurements of the sample during 10 seconds of heat flux exposure

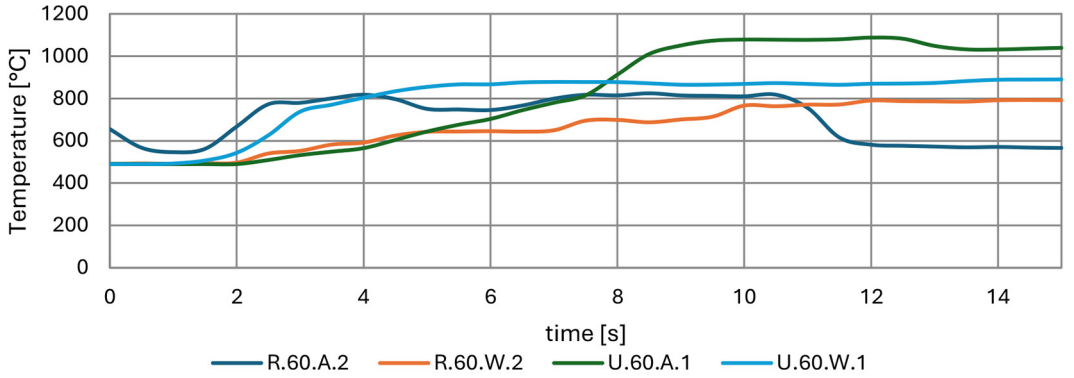

Figure 4. Results of surface temperature measurements of the sample during 15 seconds of heat flux exposure

the heated surface and the opposite surface. This behaviour results from the anisotropic nature of the laminated composite and the differing thermal conductivities of carbon and aramid fibers. Carbon fabric exhibits significantly higher thermal conductivity, whereas aramid fabric acts as a thermal insulator.

For clarity, the results were grouped into the following temperature ranges:

- 600–650 °C – heat flux applied for 5 s,
- 600–650 °C – heat flux applied for 10 s,
- 800–950 °C – heat flux applied for 15 s.

Analysis of the temperature curves indicates that the heating rate of the specimens decreases at a surface temperature of approximately 600–650 °C. For the specimens exposed to the heat flux for 5 s and 10 s, this reduced heating rate

persists until the end of the experiment, whereas specimens exposed for 15 s exhibit a rapid temperature increase, reaching up to 900–1000 °C. This behaviour is most likely associated with the onset of intensive thermal degradation of the epoxy resin, which absorbs a significant portion of the supplied energy. The specimens exposed to the heat flux for 30 s and 60 s were completely destroyed, preventing further testing. Therefore, subsequent analyses were limited to the specimens subjected to shorter exposure times, which were further evaluated through mechanical testing, surface profilometry, and optical microscopy for comparative purposes.

The results of temperature measurements on the rear surface of selected specimens are presented below. The specimen shown in Figure 5 a) was exposed to a stream of combustible gases for 5 s. A nearly linear increase in temperature up to approximately 60 °C was recorded, while the temperature on the flame-exposed side reached about 750 °C. Such a significant temperature difference indicates good thermal insulation properties; however, due to the short exposure time and a single measurement, this result is subject to considerable uncertainty.

A similar, nearly linear temperature increase was also observed for exposure times of 10 s and 15 s (Figure 5 b and c). For specimen U.30.W.1, the maximum temperature reached 98 °C (approximately 700 °C on the flame-exposed side), whereas for specimen U.60.W.1 it reached 170 °C, with about 900 °C on the flame-exposed side.

Puncture resistance test

Figure 6 presents the peak force required to penetrate the specimens as a function of heat exposure time and the surface to which the heat flux was applied.

Following the test, only a slight decrease in peak force was observed for the specimens impacted on the aramid side after thermal exposure of 5 s and 10 s (−1% and −4%, respectively). This behaviour may indicate higher thermal stability of aramid fibres. However, a significant deterioration in properties was observed after 15 s of exposure (−36%). Despite a marked reduction in puncture resistance after 15 s of thermal loading, it can be concluded that under short-term exposure to high temperatures on the aramid side, the composite largely retains its initial mechanical

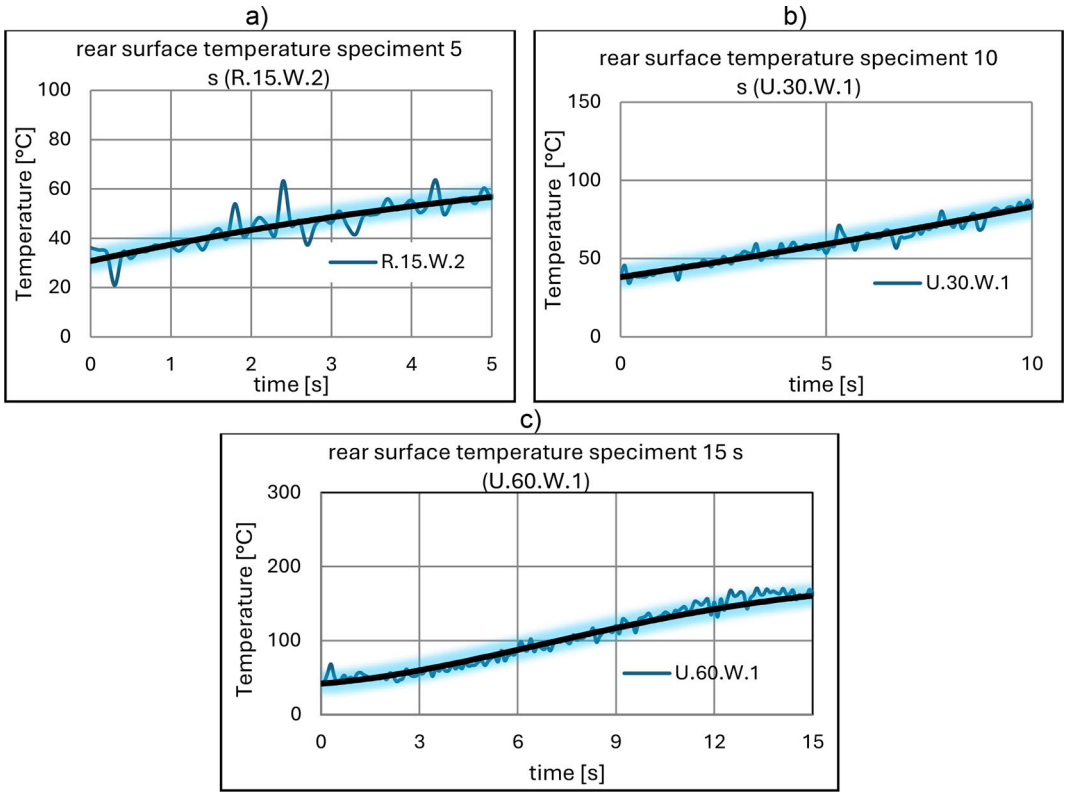

Figure 5. Results of rear surface temperature specimen during (a) 5 seconds, (b) 10 seconds and (c) 15 seconds of heat flux exposure

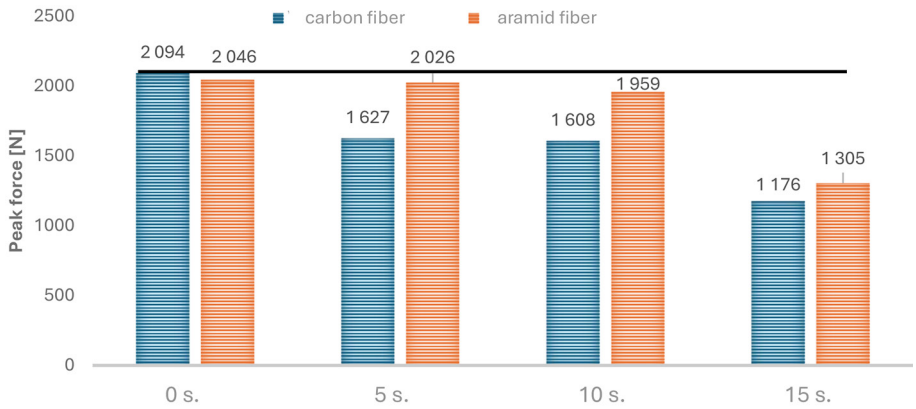

Figure 6. Peak force during impact

performance. In contrast, different behaviour was observed when the carbon layer was exposed to the heat flux. The results indicate a 22% decrease in peak force after 5 s of exposure, 23% after 10 s, and 44% after 15 s.

Static tensile test

Figure 7 shows the values of the breaking stresses for each series of specimens, illustrating the differences in strength depending on time and the side of the heat flux.

The results indicate that increasing temperature reduces tensile strength, particularly for specimens heated from the carbon side. This effect is associated with degradation of the epoxy matrix and loss of adhesion at the fibre–matrix interface. The specimens exposed to heat from the aramid side exhibit a significantly smaller reduction in tensile strength compared to those heated from the carbon side. For short exposure times (5 s and 10 s), the average decrease in ultimate tensile stress is approximately 18%, whereas for 15 s exposure it reaches 34%. In contrast, the specimens heated from the carbon side show a more pronounced reduction in strength, with decreases of 27% after 5 s, 34% after 10 s, and 53% after 15 s. These results indicate a substantially greater degradation of mechanical properties compared to the specimens exposed from the aramid side.

Figure 8 presents a comparison of the percentage elongation at break of the specimens. While the specimens exposed to heat on the aramid side show no significant change in elongation, those exposed on the carbon side exhibit a noticeable decrease. This behaviour indicates a reduction in ductility and an increased tendency for carbon fibres to fail more rapidly under elevated temperatures.

Three-point bending test

During the three-point bending test, the maximum flexural stress was determined (Figure 9).

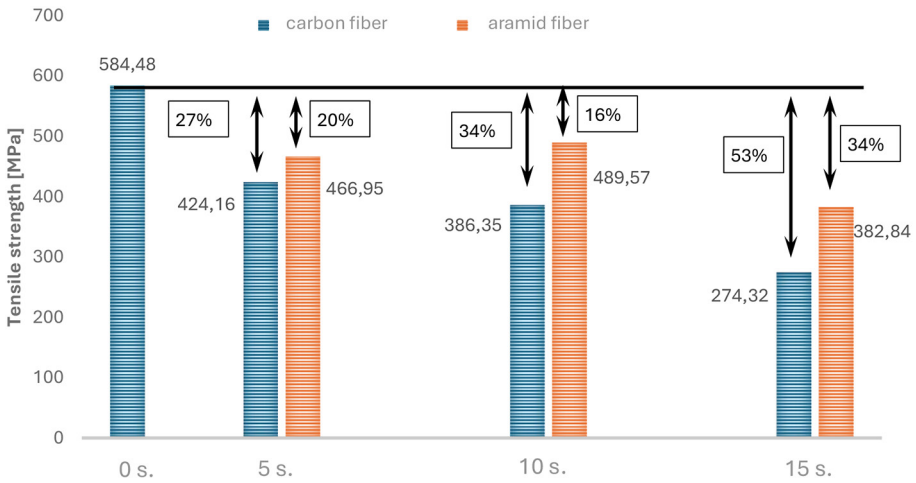

Figure 7. Summary of average values of tensile strength

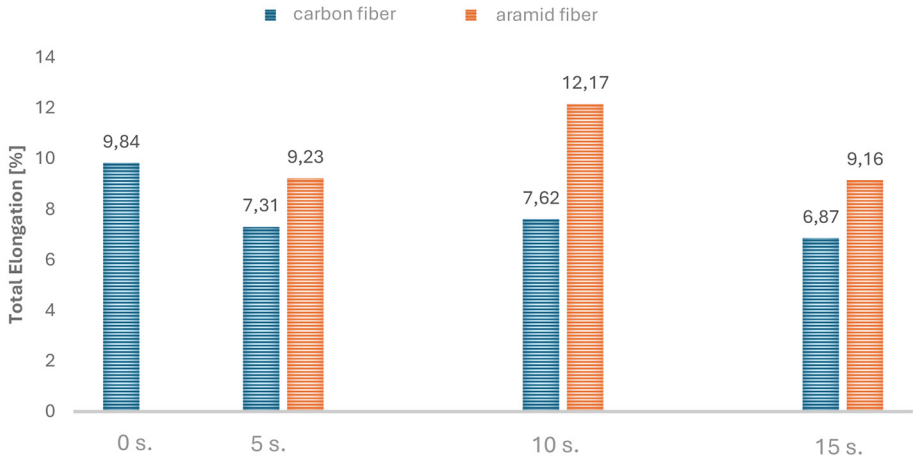

Figure 8. Summary of total elongation

A progressive degradation of mechanical properties was observed with increasing heating time. However, the layered structure of the laminate allowed it to maintain its load-bearing capacity and relatively high flexural strength only after tests lasting 5 or 10 seconds of exposure to heat. In the 15-second test, the flexural strength decreased by nearly 90%.

Microscopic analysis and structural damage

Microscopic examination of the damaged specimens confirmed the presence of:

- interlaminar delamination,
- fibre–matrix debonding in the aramid layers,
- microcracks in the matrix,
- porosity on the heated surface,
- localised charring of the structure.

Analysis of the results presented in Figures 10 and 11 indicates that the exposure to high temperatures leads to convex deformation reaching up to approximately 2 mm. This effect is most likely caused by local overheating and degradation of the matrix, accompanied by gas evolution, which promotes delamination and the formation of voids between the composite layers. A notable observation is the significant increase in surface roughness, associated with exposure of the outer carbon reinforcement layer and visible indentations across the entire sample surface. These indentations result from the weave architecture of the carbon fabric, forming in the regions between the rovings. Figures 12 and 13 present the same specimen after the puncture resistance test. No visible changes in the analysed surface were observed compared to the results shown in Figures 9–10. This behaviour can be attributed to complete degradation of the matrix bonding the outer reinforcing layers, leaving primarily a carbon fibre structure, which, due to its elastic response, returns to its original shape after impact. It should be noted

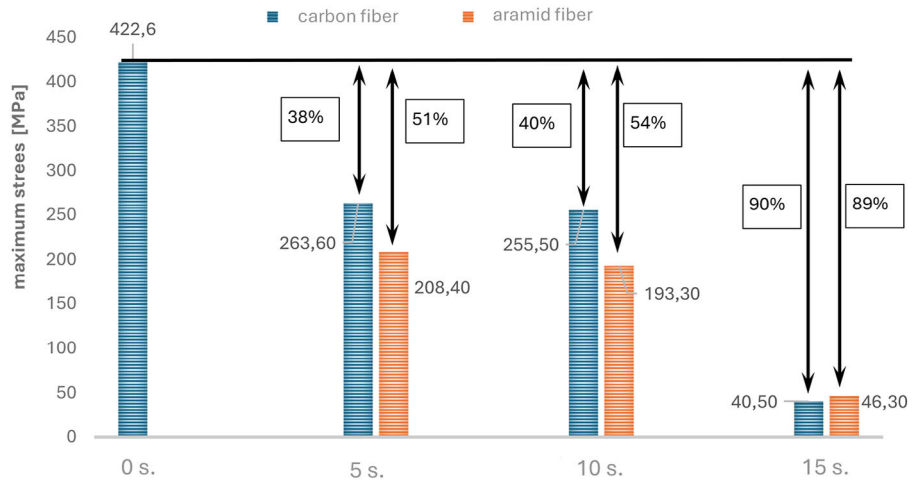

Figure 9. Comparative graph of ultimate bending stresses

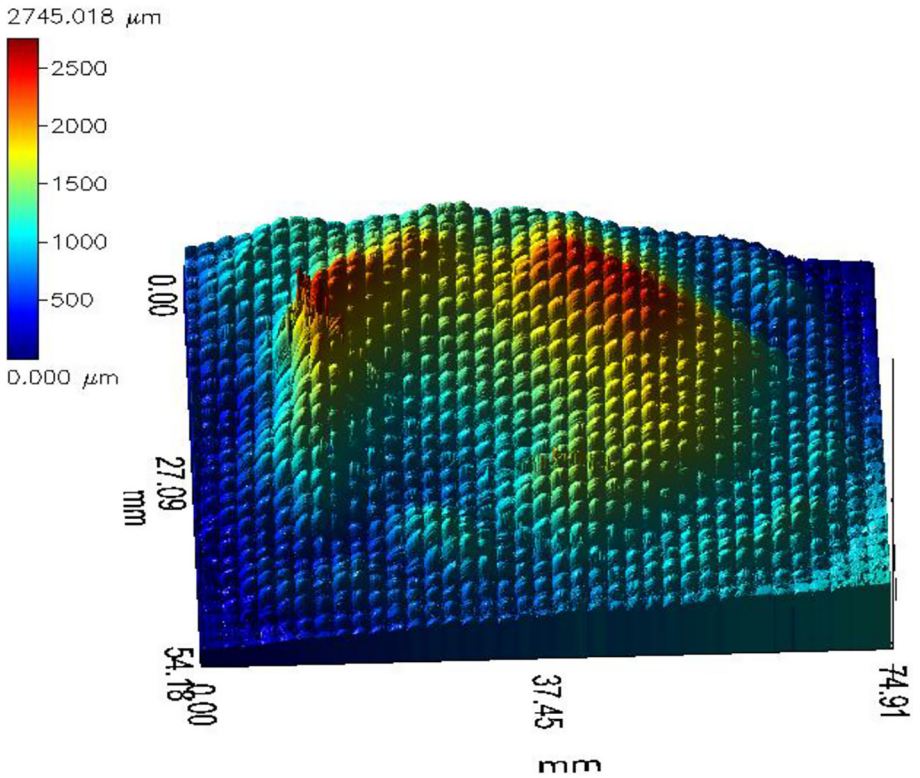

Figure 10. Three-dimensional map of the surface of the specimen U.60.W.1 topography on the side exposed to the heat flux

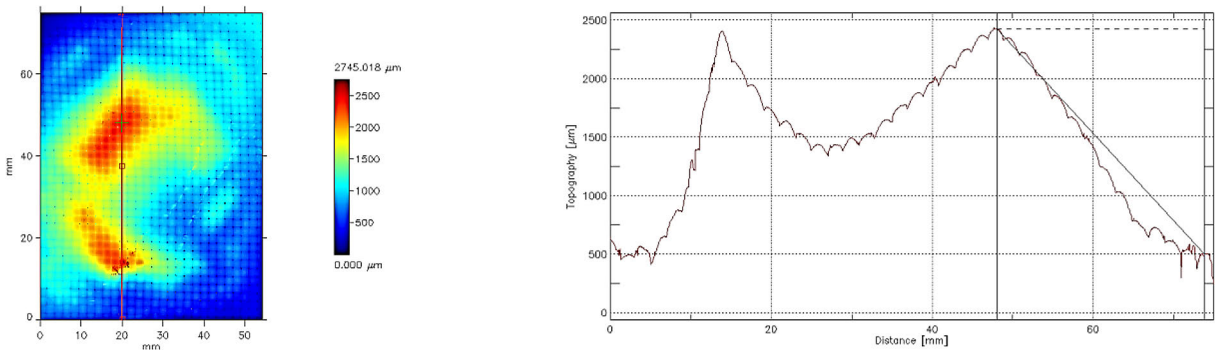

Figure 11. Profile of the sample surface height on the side exposed to the heat flux for specimen U.60.W.1

that, as a result of matrix degradation, the outer layers and likely also the second layer lose their original load-bearing capacity, thereby transferring the impact load to the underlying layers.

The profilometry results of the surface opposite to the heat-exposed side (Figures 14–15) indicate that the drop-weight impact had a significant effect on the surface geometry.

A distinct bulge, measuring approximately 0.4–0.6 mm, was observed on the scanned surface. This feature indicates the presence of microcracks and suggests a loss of structural continuity in the material. Figure 16 shows fractured carbon fibres resulting from the flexural test. Detached fragments of the reinforcing phase are clearly visible, indicating advanced structural damage of the composite.

Figure 17 illustrates the onset of cracking in the aramid fibres. The marked regions likely represent local stress concentrations that act as initiation sites for crack propagation. Detached fragments of aramid fibres and individual material particles are also visible, indicating ongoing degradation of the composite.

Figure 18 illustrates matrix degradation and the associated formation of gas bubbles. This process leads to exposure of the reinforcing phase and

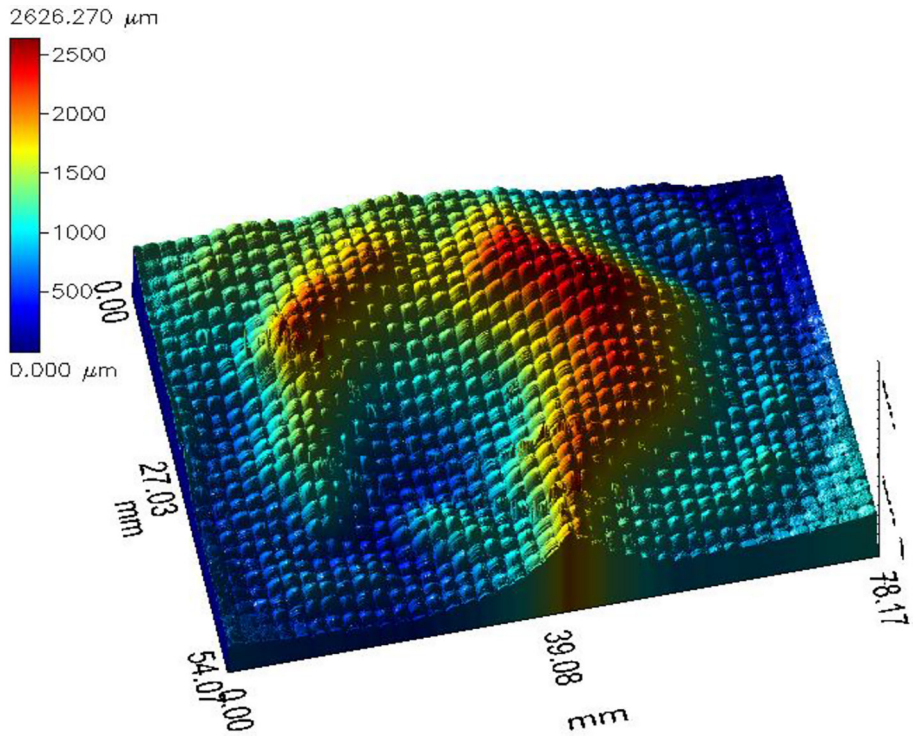

Figure 12. Three-dimensional topographic map of the surface of specimen U.60.W.1 on the side exposed to the heat flux following the puncture resistance test

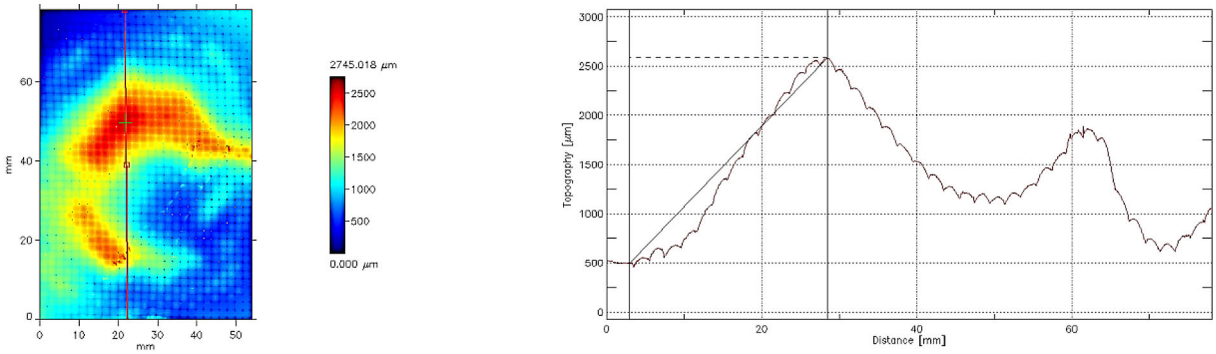

Figure 13. Profile of the surface of the specimen U.60.W.1 height on the side exposed to the heat flux after the puncture resistance test

a significant reduction in the mechanical properties of the material. Figure 19 shows cracks in the carbon fibre roving induced by high-temperature exposure. The presented region was not affected by the mechanical tests; rather, it illustrates the effect of thermal loading on the microstructure of the carbon fibre reinforcement layer.

The cross-sectional view of the specimen (Figure 20) reveals delamination of the composite induced by high-temperature exposure and bending stresses generated during testing. The resulting interlaminar voids significantly affect the static strength of the material, particularly its flexural strength.

Experimental results demonstrate that short-term exposure to a stream of hot gases leads to significant changes in the mechanical properties of the hybrid composites reinforced with carbon and aramid fibres. A clear relationship was observed between the degree of degradation, heating time, and the side of the specimen exposed to thermal loading.

The observed damage can be attributed to the interaction of the following mechanisms:

- loss of adhesion at the fibre–matrix interface,
- formation of microcracks in the epoxy matrix due to thermal stresses,

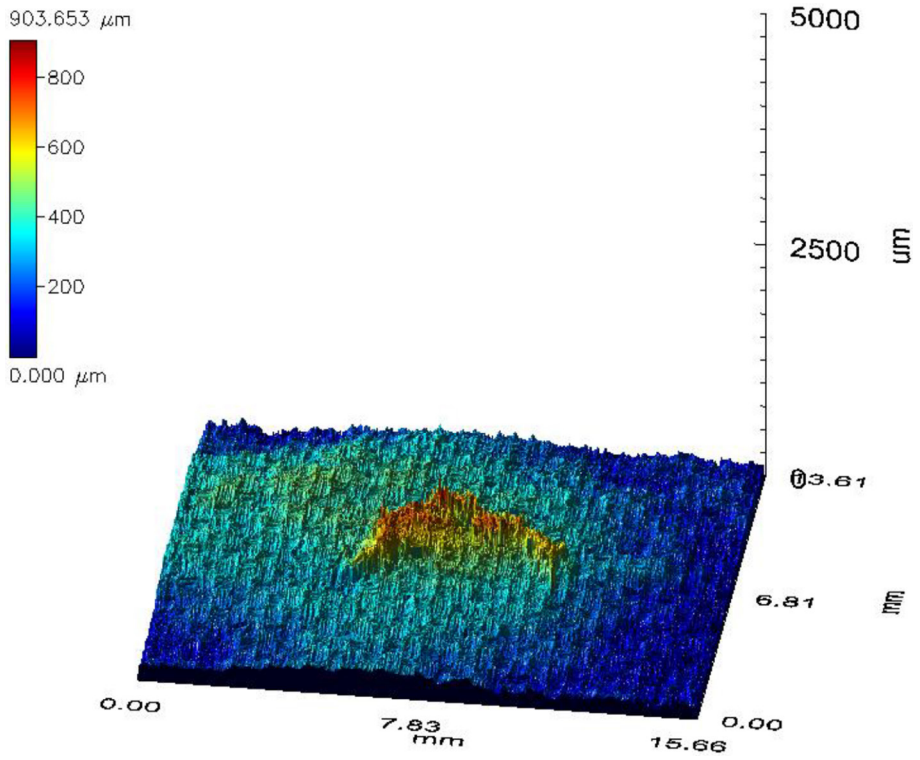

Figure 14. Three-dimensional topographic map of the surface of specimen U.60.W.1 on the opposite side after the puncture resistance test

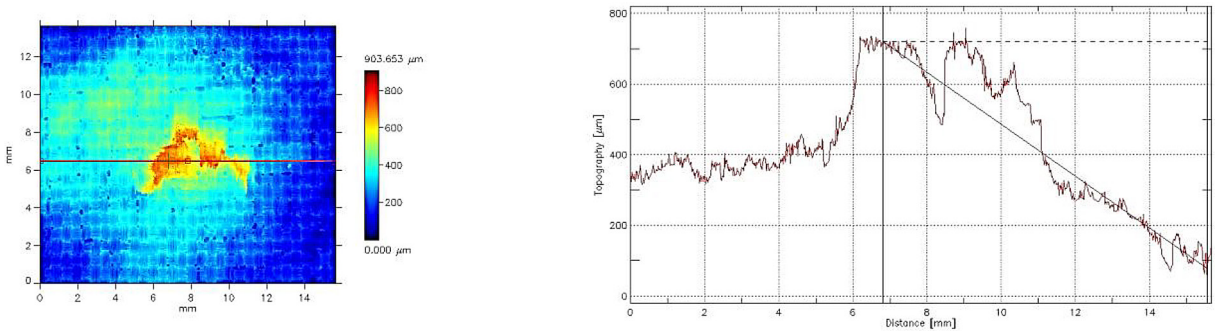

Figure 15. Profile of the surface of the specimen U.60.W.1 height on the opposite side after the puncture resistance test

- charring of surface layers as a result of resin pyrolysis,
- interlaminar delamination induced by temperature gradients,
- local loss of continuity of aramid fibres at elevated temperatures (>450 °C).

These microstructural defects lead to a progressive reduction in stiffness and load-bearing capacity of the laminate structures.

The use of a hybrid carbon–aramid composite has a significant effect on the resistance to thermal degradation of the material. Carbon fibres provide high stiffness and strength, whereas aramid fibres act as energy absorbers and thermal barriers.

The results clearly indicate that:

- the specimens heated from the aramid side retain higher mechanical properties,
- degradation propagates more slowly through the thickness,
- aramid fabrics limit delamination by enhancing stress wave damping.

These findings confirm that hybrid systems enable optimisation of the trade-off between stiffness and impact–thermal resistance.

All mechanical properties deteriorate with increasing exposure time to high temperatures. The most pronounced reduction was observed in impact tests, which is attributed to degradation of

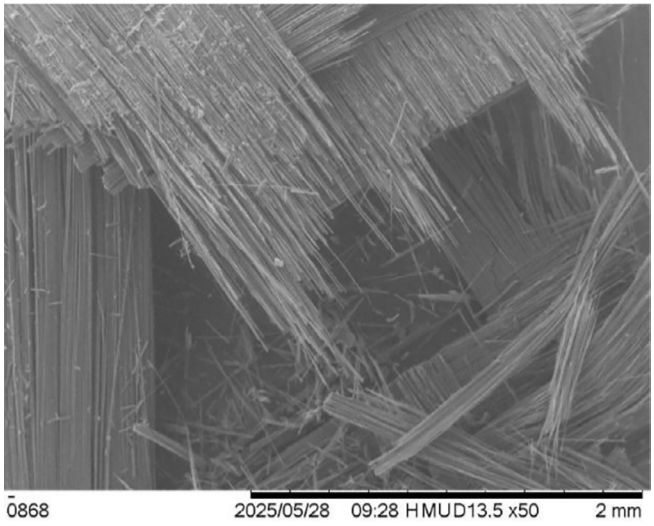

Figure 16. Specimen Z.60.W.2, SEM–EDX method, SE detection mode, 50× magnification

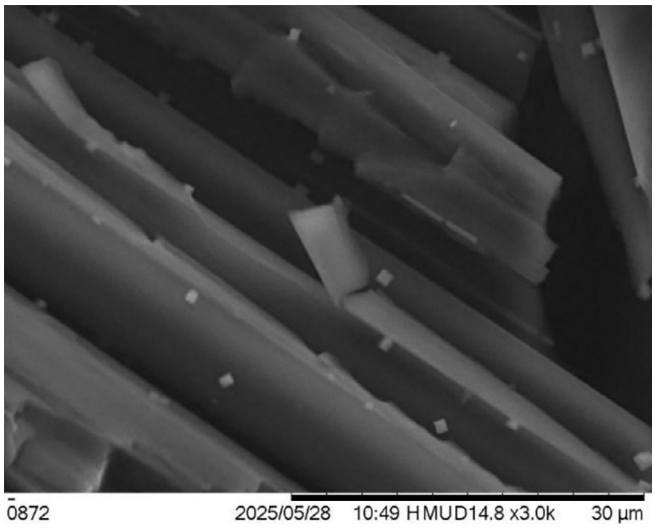

Figure 17. Specimen Z.60.A.3, SEM–EDX method, SE detection mode, magnification ×3000

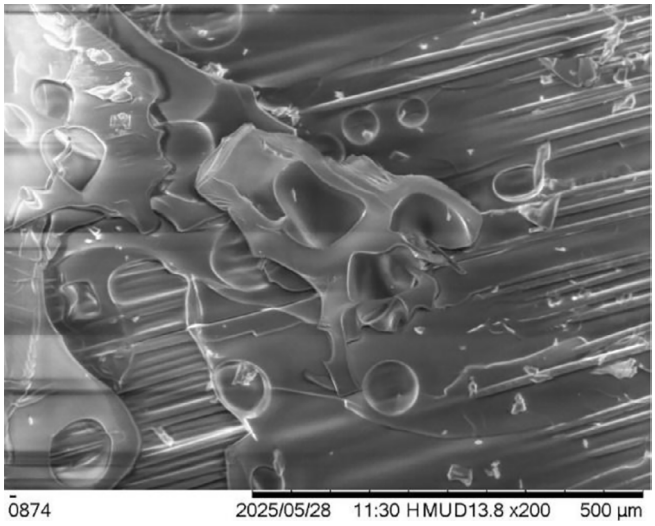

Figure 18. Specimen Z.60.A.3, SEM–EDX method, SE detection mode, magnification ×200

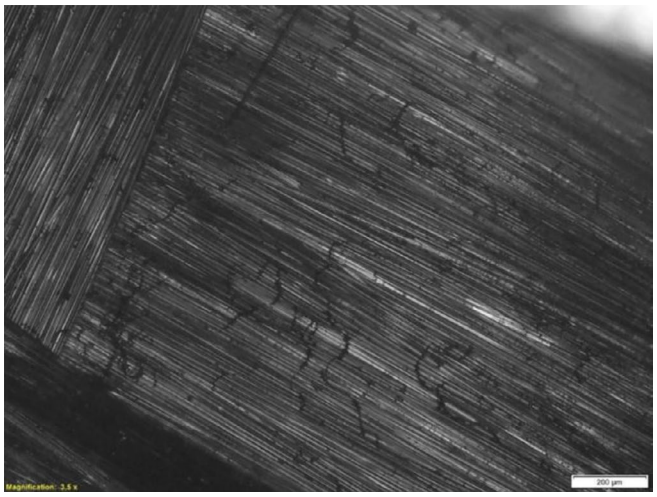

Figure 19. Specimen Z.60.W.3, magnification x5, cracks in the aramid fibres

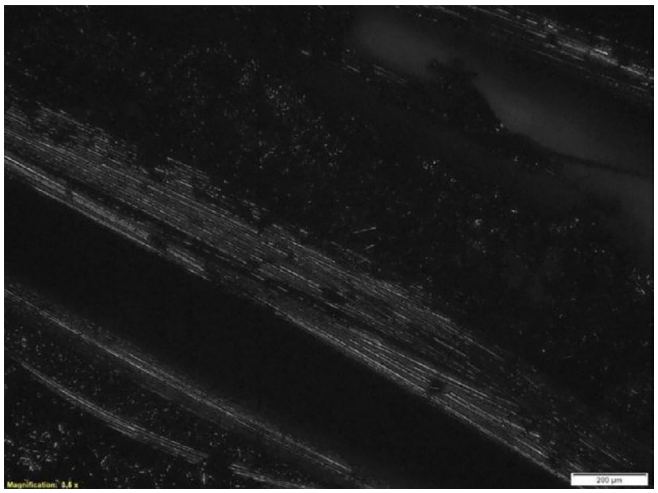

Figure 20. Cross-section of specimen Z.60.W.3, magnification x5, delamination of the composite

the matrix structure while the reinforcing fibres remain largely intact. In tensile testing, the dominant mechanisms include interlaminar delamination and interfacial slippage.

The results of this study are of significant importance for the design of structural components exposed to flame or high-temperature environments, such as:

- ballistic shields for military vehicles,
- engine compartments in aerospace applications,
- protective panels in unmanned aerial vehicle (UAV) systems,
- hull structures of patrol boats,
- ammunition storage and protection containers.

From a structural safety perspective, the findings indicate that the greatest risk of loss of load-bearing capacity occurs under bending and impact loading following thermal exposure. The results highlight the necessity of incorporating protective layers and ablative barriers in composites intended for operation under extreme conditions.

CONCLUSIONS

The exposure to high temperatures causes a rapid decline in the mechanical properties of composites, which becomes apparent after just a few seconds and worsens over time. Greater degradation is observed when heating from the carbon fibre side rather than the aramid fibre side. Flexural strength and impact strength are the most sensitive, indicating a predominance of interlaminar damage; in the case of flexural strength, the decrease reaches ~90%. The use of hybrid carbon-aramid reinforcement improves thermal resistance due to the thermal barrier effect of the

aramid fibres. Degradation includes charring, microcracks, loss of adhesion, and delamination. Future research include:

- implementation of sacrificial protective layers,
- investigation of degradation under thermal fatigue conditions,
- application of dynamic mechanical analysis (DMA) and thermogravimetric analysis (TGA) to evaluate matrix behaviour,
- numerical modelling of thermomechanical degradation processes.

REFERENCES

1. Szczepaniak R., Przybyłek P., Krzysztofik K. Effect of the amount and location of phase change materials in a fibre reinforced composite matrix on ablative properties, Adv. Sci. Technol. Res. J. 2025, 19(3), 228–237. https://doi.org/10.12913/22998624/196965
2. Przybyłek P., Komorek A., Szczepaniak R. the influence of metal reinforcement upon the ablative properties of multi-layered composites, Adv. Sci. Technol. Res. J. 2023, 17(2), 111–119. https://doi.org/10.12913/22998624/161427
3. Natali M., Kenny J.M. Science and technology of polymeric ablative materials for thermal protection systems and propulsion devices: A review, Progress in Materials Science, 2016, 84, 192–275. https://doi.org/10.1016/j.pmatsci.2016.08.003
4. Xing X., Zhao Y. Healable ablative composites from synergistically crosslinked phenolic resin, Chemical Engineering Journal, 2022, 447, 137571. https://doi.org/10.1016/j.cej.2022.137571
5. Colonel V. K. Polymer Composites as Ablative Materials, Macromolecular Engineering: From Precise Synthesis to Macroscopic Materials and Applications, 2022, Publisher: WILEY. https://doi.org/10.1002/9783527815562.mme0039
6. Bakar M., Kucharczyk W., Stawarz S. Investigation of thermal and ablative properties of modified epoxy resins. Polym. Polym. Compos. 2016, 24(8), 617–623.
7. Wang C. Numerical analyses of ablative behavior of C/C composite, International Journal of Heat and Mass Transfer 2016, 95, 720–726. https://doi.org/10.1016/j.ijheatmasstransfer.2015.12.031
8. Lachaud J. A short review of ablative-material response models and simulation tools, 7th Aerothermodynamics Symposium (European Space Agency), Site Oud Sint-Jan, Brugge, Belgium 2011, Session: Thermal Protection Systems.
9. Boyd M. Simulation of pyrolysis gas within a thermal protection system. In AIAA, editor, 40thThermophysics Conference, Seattle, Washington 2008 3805, 20.
10. Li W., Fang G., Numerical simulation of microablation behavior for carbon fiber reinforced composites, Chinese Journal of Theoretical and Applied Mechanics, 2019, 51(3), 835–844. https://doi.org/10.6052/0459-1879-18-351
11. Yadav R. The role of fillers to enhance the mechanical, thermal, and wear characteristics of polymer composite materials: A review, Composites Part A: Applied Science and Manufacturing 2023, 175, 107775. https://doi.org/10.1016/j.compositesa.2023.107775
12. Zhang H. A thermo-chemo-mechanical damage model for carbon/carbon composites under ablative conditions: application to short fiber reinforced microstructures, Carbon 2025, 244, 120703. https://doi.org/10.1016/j.carbon.2025.120703
13. Szczepaniak R., Kozun G. The effect of the application of a powder additive of a phase change material on the ablative properties of a hybrid composite, Composite Structures 2021, 256, 113041. https://doi.org/10.1016/j.compstruct.2020.113041
14. Kang O., Zhongguo L. Effect of (Hf, Zr, Nb, Ti)C high-entropy ceramic powders on ablation property of C/C-(Hf, Zr, Nb, Ti)C-SiC composites and its ablative mechanism under long time ablation, Journal of Alloys and Compounds 2025, 1041, 183698. https://doi.org/10.1016/j.jallcom.2025.183698
15. Cao J. Tribology and anti-ablation properties of SiC-VN-MoS2/Ta composite coatings on carbon/carbon composites from 25 to 800 °C, Materials 2021, 14, 6772. https://doi.org/10.3390/ma14226772
16. Liu F.H., Yi M.Z., Ran L.P., Ge Y.C., Peng K. Influence of preparation method on microstructure and tribo-logical behavior of C/C-BN composites. Ceram. Int. 2021, 47, 12879–12896. https://doi.org/10.1016/j.ceramint.2021.01.151
17. Zhang R., Ding Q., Zhang S., Li Y., Niu Q., Yang L., Ye J., Hu L. The effects of ultrasonication on the microstructure, gelling and tribological properties of 12-HSA soft-nanocomposite with LaF3 nanoparticles. Colloids Surf. A Physicochem. Eng. Asp. 2019, 586, 124247. https://doi.org/10.1016/j.colsurfa.2019.124247
18. Badea T.A. Enhanced ablative performance of additively manufactured thermoplastic composites for lightweight thermal protection systems (TPS), Polymers 2025, 17(18), 2462. https://doi.org/10.3390/polym17182462
19. Ling Y., Xiao B. Green surface modification strategy: Synergistic carboxymethyl cellulose -SiO2 hybrid layer boosts interfacial and ablative properties of aramid fiber/EPDM composites, Composites Science and Technology 2025, 269, 18, 111241. https://doi.org/10.1016/j.compscitech.2025.111241

20. Kumar C.V. Advances in ablative composites of carbon based materials: A review, Ind. Eng. Chem. Res. 2019, 58, 51, 22663–22701. https://doi.org/10.1021/acs.iecr.9b04625
21. John B. Phenolic syntactic foams: Low-density composites for structural and thermostructural applications, Cellular Polymers 2022, 41, 5. https://doi.org/10.1177/02624893221101147
22. Wu X., Ding J., Kong Y., Sun Z., Shao G., Li B., Wu J., Zhong Y., Shen X., Cui S. Synthesis of a novel three-dimensional Na2SO4@SiO2@Al2O3-SiO2 phase change material doped aerogel composite with high thermal resistance and latent heat. Ce ram. Int., 2018, 44(17), 21855–21865. https://doi.org/10.1016/j.ceramint.2018.08.294
23. He F., Wang X., Wu D. Phase-change characteristics and thermal performance of form-stable n-alkanes/silica composite phase change materials fabricated by sodium silicate precursor. Renewable Energy. 2015, 74, 689–698. https://doi.org/10.1016/j.renene.2014.08.079
24. Panas A.J., Szczepaniak R., Stryczniewicz W., Omen Ł. Thermophysical properties of pressure sensitive pain, Thermochimica Acta, 2023, 730, 179612, https://doi.org/10.1016/j.tca.2023.179612 27
25. Krzyżak A., Relich S., Kosicka E., Szczepaniak R., Mucha M. Selected construction properties of hybrid epoxy composites reinforced with carbon fiber and alumina. Adv. Sci. Technol. Res. J. 2022, 16(2). https://doi.org/10.12913/22998624/147521
26. Yang J., Ji C., Wang D., Zhang H., Zhou Z., Hu J., Wang B. Fire behavior and post-fire residual tensile strength prediction of carbon fiber/phthalonitrile composite laminates, Compos. Sci. Technol., 2024, 252, 110624. https://doi.org/10.1016/j.compscitech.2024.110624
27. Yang J., Wang D., Hu J., Ji C., Wang B. Residual tensile behavior of carbon fiber/phthalonitrile composites after isothermal and anisothermal heating, Composites Communications, 2025, 57, 102429. https://doi.org/10.1016/j.coco.2025.102429
28. Aspinall T.J., Erskine E.L., Taylor D.C., Hadden R.M. Effect of fibre orientation and thermal exposure on the post-fire mechanical behaviour of carbon fibre reinforced polymer material, Fire and Materials, 2023. https://doi.org/10.1002/fam.3163
29. Xu F., Sha Z., Zhuo L., Chang W., Sun B., Wang C.H., Gu B., Zhang J. Improving thermal stability and mechanical properties of high temperature carbon fibre phthalonitrile resin composites via Nano-CuO modified matrices, Composites Part A: Applied Science and Manufacturing, 2025, 197, 109035, https://doi.org/10.1016/j.compositesa.2025.109035